Wave Attenuation and Wave Drift in the Marginal Ice Zone

JAN ERIK WEBER

Institute of Geophysics, University of Oslo, 0315 Oslo 3, Norway

(Manuscript received 17 February 1987, in final form 22 May 1987)

ABSTRACT

Surface gravity waves in a viscous rotating ocean are studied theoretically when they penetrate an area covered by highly concentrated brashlike ice. The motion is described by a Lagrangian formulation, and the brash is modeled by a viscous Newtonian fluid. Results for wave attenuation and wave drift are obtained in the asymptotic limit of a thin, very viscous upper layer. The derived damping rate compares favorably with field data from the marginal ice zone (MIZ). The drift velocity in the ocean exhibits a marked maximum in the viscous boundary layer near the ice–ocean interface. At the outer edge of the boundary layer it exceeds the inviscid Stokes drift by a factor of 7/4. Computed values for the mean viscous drag on the ice induced by the wave motion show that this effect may compete with the frictional effect of the wind in packing the ice. Finally it is demonstrated that the integrated horizontal mass transports in the open ocean and under the ice do not match, which leads to upwelling in the vicinity of the ice edge.

1. Introduction

The fact that ocean waves attenuate when they penetrate areas covered by ice floes is well established. The loss of wave energy is attributed to the presence of the ice and depends on ice concentration, floe size, etc. These parameters, in turn, depend on the energy and characteristics of the incident wave field, because floes tend to break up if they are too large to exist in the local wave climate. The area in which this complicated wave–ice interaction occurs is known as the marginal ice zone (MIZ). Ice conditions are not uniform within the MIZ, and it is often divided into three subzones: the edge zone, the transition zone and the interior zone (Squire and Moore, 1980; Squire, 1983a). Each zone is characterized by ice floes of a certain size; the size increases moving inward from the ice edge.

Constructing a general model for wave attenuation in the MIZ is a formidable task, due to the rather inhomogeneous conditions encountered by the waves as they penetrate the ice-covered area. Furthermore, within the previously defined subzones, the ice conditions may vary with geographical location and local meteorological conditions. This is particularly evident in the edge zone, often taken to be part of the MIZ within 5 km or so off the ice edge. Here the ice is most directly exposed to the action of the waves, and the floe size and ice configuration may vary considerably.

The only theories so far to explain the loss of wave energy in the ice are wave scattering by individual ice floes (Wadhams, 1973a, 1975) and inelastic bending of the ice sheet (Wadhams, 1973b; Squire, 1978). Single scattering theory requires that the reflected energy is dissipated before reaching the preceding floe, i.e., it assumes that the ice floes are rather far apart. Multiple scattering allows a wave vector to be reflected twice before dissipating, and is therefore a better approximation for higher ice concentrations. Inelastic bending is probably only important for very large ice floes or fast ice. However, it is not uncommon to find situations in the MIZ where the ice floes are quite small and rather densely packed. The occurrence of brash ice at the extreme ice edge is such an example (Squire, 1984). Here the ice floes have been broken down to a highly concentrated brashlike viscous soup of small ice cakes. Grease ice is a second example. It is formed from frazil ice in the presence of wind (Martin and Kauffman, 1981) and constitutes a soupy agglomeration layer of thickness up to one meter.

Until now the effect of viscosity has been neglected in the various attempts to explain the attenuation of surface waves in the pack ice. However, it seems rather unlikely that this effect should not play an important role in determining the high attenuation rates observed in ice configurations like those mentioned above. To simplify the problem, we assume that the "soupy" ice-agglomeration behaves like a Newtonian fluid. Physically, the problem is then reduced to that of analyzing the propagation of gravity waves in a rotating, slightly viscous ocean covered by a thin layer of very viscous fluid. Since most ocean waves have wavelengths λ much larger than the thickness h of the ice-agglomeration layer, results will be obtained only in the asymptotic limit $h/\lambda \ll 1$.

Although our theoretical analysis is based on a special type of ice, we find that our model in fact does apply to more general conditions encountered within the MIZ. This is evident from a good fit between the theory and observational data from various attenuation measurements in the pack ice.

A nonlinear analysis is performed to second order in wave amplitude, and the wave-induced drift current (the mean mass transport) below the ice layer is determined, which enables us to calculate the mean viscous stresses exerted on the ice. The importance of this mechanism in packing the ice is discussed. Finally, we demonstrate that the integrated wave-induced mass transport attains different values in the open ocean and under the ice. This must inevitably lead to upwelling near the ice edge.

2. Mathematical formulation

We consider an unlimited ocean of infinite depth partly covered by a thin, very viscous fluid layer of thickness h. The system rotates about the vertical axis with a constant angular velocity $f/2$, where f is the Coriolis parameter. A Cartesian right-handed coordinate system is defined such that the x, y-axes are situated at the undisturbed interface between the two fluids. The z-axis is directed vertically upwards. We consider only positive values of x, i.e. we place the ice edge at $x = 0$; see the sketch in Fig. 1. The ice-agglomeration layer and the ocean, labeled 1 and 2 respectively, are both taken to be homogeneous, incompressible Newtonian fluids.

We describe the motion in each layer by using a Lagrangian formulation. This proves very convenient in problems involving freely undulating material surfaces (Weber, 1983a,b). Let a fluid particle have coordinates (a, b, c) at time $t = 0$. At later times it occupies the position (x, y, z). The governing equations for momentum and mass in each layer may then be written:

$$\left.\begin{aligned} x_{tt} - fy_t &= -\frac{1}{\rho}\frac{\partial(p,y,z)}{\partial(a,b,c)} + \nu\nabla^2 x_t \\ y_{tt} + fx_t &= -\frac{1}{\rho}\frac{\partial(x,p,z)}{\partial(a,b,c)} + \nu\nabla^2 y_t \\ z_{tt} + g &= -\frac{1}{\rho}\frac{\partial(x,y,p)}{\partial(a,b,c)} + \nu\nabla^2 z_t \end{aligned}\right\} \tag{2.1}$$

$$\frac{\partial(x,y,z)}{\partial(a,b,c)} = 1. \tag{2.2}$$

Here p denotes the pressure, ρ the density, ν the kinematic viscosity and g the acceleration due to gravity.

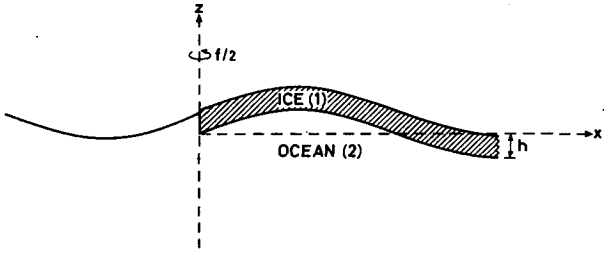

FIG. 1. Model sketch.

Subscripts denote partial differentiation and $\partial/\partial(a, b, c)$ is the Jacobian. For the explicit form of the Laplacian ∇^2 in Lagrangian form, the reader is referred to Pierson (1962).

The displacements (x, y, z) and pressure p in each layer will be written as series expansions (Pierson, 1962):

$$\left.\begin{aligned} x_{1,2} &= a + \epsilon x_{1,2}^{(1)} + \epsilon^2 x_{1,2}^{(2)} + \cdots \\ y_{1,2} &= b + \epsilon y_{1,2}^{(1)} + \epsilon^2 y_{1,2}^{(2)} + \cdots \\ z_{1,2} &= c + \epsilon z_{1,2}^{(1)} + \epsilon^2 z_{1,2}^{(2)} + \cdots \\ p_1 &= -\rho_1 g(c-h) + \epsilon p_1^{(1)} + \epsilon^2 p_1^{(2)} + \cdots \\ p_2 &= \rho_1 gh - \rho_2 gc + \epsilon p_2^{(1)} + \epsilon^2 p_2^{(2)} + \cdots \end{aligned}\right\} \tag{2.3}$$

Here ϵ is an ordering parameter proportional to the amplitude of the wave. The position of the upper boundary of the ice is given by $c = h$ for all times, while the ice–ocean interface is given by $c = 0$. Accordingly, label $^{(1)}$ refers to the domain $0 \leqslant c \leqslant h$, while label $^{(2)}$ refers to $c \leqslant 0$.

For future reference we state the horizontal and vertical dynamic stresses $P^{(xz)}$ and $P^{(zz)}$ at a sloping material surface c = constant. We consider wave propagation along the x-axis. Hence $\partial/\partial b = 0$ in the perturbations. For reasons which become obvious in the next section, we put $y_{1,2}^{(1)} = 0$. Utilizing series expansions of the type (2.3), we then obtain

$$\begin{aligned} P^{(xz)} = \epsilon\mu[x_{tc}^{(1)} + z_{ta}^{(1)}] + \epsilon^2[&p^{(1)} z_a^{(1)} + \mu(x_{tc}^{(2)} + z_{ta}^{(2)} \\ &+ x_a^{(1)} x_{tc}^{(1)} - x_{ta}^{(1)} x_c^{(1)} + z_{ta}^{(1)} z_c^{(1)} - z_a^{(1)} z_{tc}^{(1)} - 2x_{ta}^{(1)} z_a^{(1)})] \\ &+ \mathrm{O}(\epsilon^3) + \cdots, \quad c = \text{const} \end{aligned} \tag{2.4}$$

$$\begin{aligned} P^{(zz)} = \epsilon[-p^{(1)} + 2\mu z_{tc}^{(1)}] + \epsilon^2[&\\ &-p^{(2)} + \mu(2z_{tc}^{(2)} + 2x_a^{(1)} z_{tc}^{(1)} \\ &- 2x_c^{(1)} z_{ta}^{(1)} - x_{tc}^{(1)} z_a^{(1)} - z_{ta}^{(1)} z_a^{(1)})] + \mathrm{O}(\epsilon^3) + \cdots, \\ &c = \text{const}. \end{aligned} \tag{2.5}$$

Here $\mu = \rho\nu$ is the dynamic viscosity coefficient. For further details concerning the conditions above, see Chang (1969) and Weber (1983a, 1985).

3. Linear analysis for upper layer

The linear solution is obtained by inserting the expansions (2.3) into (2.1) and (2.2), collecting terms proportional to ϵ. We assume that the viscosity of the upper layer is so large that the motion here essentially results from a balance between pressure and friction (creeping motion). Hence for motion in the x, z-plane with $y_1^{(1)} = 0$, the continuity equation (2.2) is satisfied by a streamfunction $\psi_1^{(1)}$ such that

$$x_{1t}^{(1)} = \psi_{1c}^{(1)}, \quad z_{1t}^{(1)} = -\psi_{1a}^{(1)}. \tag{3.1}$$

The momentum balance (2.1) then leads to the familiar biharmonic equation for $\psi_1^{(1)}$:

$$\nabla_L^4 \psi_1^{(1)} = 0 \tag{3.2}$$

where $\nabla_L^2 = \partial^2/\partial a^2 + \partial^2/\partial c^2$. We assume that the waves propagate in the x-direction, and take

$$\psi_1^{(1)} = \Psi(c) e^{i(\kappa a - \omega t)} \tag{3.3}$$

where the wavenumber κ and the frequency ω in principle may be complex. Equation (3.2) is satisfied by a solution of the form

$$\Psi = (A_1 + A_2 c)e^{\kappa c} + (A_3 + A_4 c)e^{-\kappa c} \tag{3.4}$$

where the As are constants.

We assume that the atmospheric pressure along the surface of the upper layer is constant. Furthermore, the stresses are taken to be zero here, i.e., we ignore any viscous effects of the air. From (2.4) and (2.5) the requirement of vanishing horizontal and vertical stresses to $O(\epsilon)$ at the free surface reduce to

$$\left.\begin{aligned} \Psi_{cc} + \kappa^2 \Psi = 0 \\ \Psi_{ccc} - 3\kappa^2 \Psi_c - 2\kappa^3 Q \Psi = 0 \end{aligned}\right\}, \quad c = h. \tag{3.5}$$

Here Q is a dimensionless parameter defined by

$$Q = \frac{ig}{2\nu_1 \omega \kappa}. \tag{3.6}$$

Utilizing (3.5), we may express A_3 and A_4 in (3.4) as functions of A_1 and A_2.

We have assumed that the viscosity of the ice-agglomeration layer is very large. This means that we take $|Q| \ll 1$. Furthermore, we assume that the upper layer thickness h is small compared to the wavelength, i.e. $|\kappa h| \ll 1$, which proves to be a very reasonable approximation. Usually brash- or grease-ice layers have thicknesses less than one meter, while the most energetic ocean waves penetrating the ice may have periods of 10 sec or more. This corresponds to wavelengths well above 100 m.

To lowest order in the small parameters Q and κh, the velocity components and stress distributions at the bottom of the brash-ice layer may be written:

$$\left.\begin{aligned} x_{1t}^{(1)} &= -\kappa A_0 \exp[i(\kappa a - \omega t)] \\ z_{1t}^{(1)} &= -2i\kappa A_1 \exp[i(\kappa a - \omega t)] \\ P_1^{(xz)}/\epsilon &= 4\kappa^2 \mu_1 (\kappa h) A_0 \exp[i(\kappa a - \omega t)] \\ P_1^{(zz)}/\epsilon &= 2i\kappa^2 \mu_1 (\kappa h)(\kappa h - Q) A_0 \exp[i(\kappa a - \omega t)] \end{aligned}\right\}, \quad c = 0. \tag{3.7}$$

where we have defined $A_0 = -2(A_1 + A_2/\kappa)$.

4. Linear analysis for lower layer

We consider high-frequency gravity waves, i.e. $|\omega| \gg f$. The effect of rotation can be neglected to $O(\epsilon)$ for the ocean wave problem (Weber, 1986). For waves propagating in the x-direction, $y_2^{(1)} \approx 0$ in the solutions. The ocean is assumed to be only slightly viscous, and a solution to the wave problem may be obtained along the lines of Lamb (1932). Defining

$$\left.\begin{aligned} x_{2t}^{(1)} &= -\varphi_{2a}^{(1)} - \psi_{2c}^{(1)} \\ z_{2t}^{(1)} &= -\varphi_{2c}^{(1)} + \psi_{2a}^{(1)}, \end{aligned}\right\} \tag{4.1}$$

the linearized versions of (2.1) and (2.2) reduce to

$$\left.\begin{aligned} \nabla_L^2 \varphi_2^{(1)} &= 0 \\ \psi_{2t}^{(1)} - \nu_2 \nabla_L^2 \psi_2^{(1)} &= 0. \end{aligned}\right\} \tag{4.2}$$

The pressure $p_2^{(1)}$ is obtained from

$$p_2^{(1)} = \rho_2 \varphi_{2t}^{(1)} - \rho_2 g z_2^{(1)}. \tag{4.3}$$

The solutions are:

$$\left.\begin{aligned} x_2^{(1)} &= \frac{1}{i\omega}[i\kappa B_1 e^{\kappa c} + m B_2 e^{mc}] e^{i(\kappa a - \omega t)} \\ z_2^{(1)} &= \frac{1}{i\omega}[\kappa B_1 e^{\kappa c} - i\kappa B_2 e^{mc}] e^{i(\kappa a - \omega t)} \\ p_2^{(1)} &= \left[\frac{i\rho_2}{\omega}(g\kappa - \omega^2) B_1 e^{\kappa c} + \frac{\rho_2 g \kappa}{\omega} B_2 e^{mc}\right] e^{i(\kappa a - \omega t)} \end{aligned}\right\} \tag{4.4}$$

where $m^2 = \kappa^2 - i\omega/\nu_2$. Here we have assumed that $\mathrm{Re}(\kappa) > 0$ in order that the solutions vanish as $c \to -\infty$.

If ν_2 is small, one obtains approximately (Lamb, 1932):

$$m = (1 - i)\left[\frac{\mathrm{Re}(\omega)}{2\nu_2}\right]^{1/2} \equiv (1 - i)\gamma. \tag{4.5}$$

We note that γ^{-1} defines the thickness of the viscous boundary layer in the ocean below the interface $c = 0$.

The velocities and dynamic stresses in the ocean at the interface may then be written:

$$\left.\begin{aligned} x_{2t}^{(1)} &= [-i\kappa B_1 - m B_2] \exp[i(\kappa a - \omega t)] \\ z_{2t}^{(1)} &= [-\kappa B_1 + i\kappa B_2] \exp[i(\kappa a - \omega t)] \\ P_2^{(xz)}/\epsilon &= \mu_2[-2i\kappa^2 B_1 - (m^2 + \kappa^2) B_2] \exp[i(\kappa a - \omega t)] \\ P_2^{(zz)}/\epsilon &= \left[-\left(\frac{i\rho_2 g\kappa}{\omega} - i\rho_2 \omega + 2\mu_2 \kappa^2\right) B_1 + \left(-\frac{\rho_2 g \kappa}{\omega}\right.\right. \\ &\quad \left.\left. + 2i\mu_2 \kappa m\right) B_2\right] \exp[i(\kappa a - \omega t)] \end{aligned}\right\}, \quad c = 0. \tag{4.6}$$

In general, the dispersion relation and the integration constants are determined from (3.7) and (4.6) by requiring continuity of velocities and stresses at the interface $c = 0$. The solutions may be normalized by taking $B_1 = 1$. Continuity of the horizontal velocities leads to

$$A_0 = i + m B_2/\kappa. \tag{4.7}$$

Hence the conditions for continuity of horizontal and vertical stresses at $c = 0$ may be written:

$$[(\kappa^2 + m^2)\mu_2 + 4\kappa m\mu_1\kappa h]B_2 = -2i\kappa^2(\mu_2 + 2\mu_1\kappa h) \quad (4.8)$$

$$\left[\frac{g}{\omega}(\rho_2\kappa + \rho_1 m\kappa h) - 2i\kappa m\mu_2 + 2i\kappa m\mu_1\kappa^2 h^2\right]B_2$$

$$= i\rho_2\omega - \frac{ig\kappa}{\omega}(\rho_2 + \rho_1\kappa h) - 2\kappa^2\mu_2 + 2\kappa^2\mu_1\kappa^2 h^2. \quad (4.9)$$

Finally, the dispersion relation may be obtained by the elimination of B_2 between (4.8) and (4.9).

Since the wave amplitude is observed to diminish as the wave propagates inwards from the ice edge, the decay here is most naturally described as a spatial one. Accordingly, we take ω to be real, place the ice edge at $x = 0$ (Fig. 1) and restrict ourselves to the half-plane $x \geq 0$. Spatial attenuation then means that κ is complex and such that $\mathrm{Im}(\kappa) > 0$. Also, as mentioned before, $\mathrm{Re}(\kappa) > 0$, to ensure that our solutions vanish as $c \to -\infty$.

For the problem considered here, we assume that μ_1 is very large and μ_2 small. The latter requirement means that

$$|m| = (\omega/\nu_2)^{1/2} \gg |\kappa|. \quad (4.10)$$

If we now assume that μ_1 is so large that

$$|m\mu_2| \ll |4\kappa\mu_1(kh)|, \quad (4.11)$$

we obtain from (4.8) that

$$B_2 \approx -i\kappa/m. \quad (4.12)$$

As seen from (4.6) this implies that $x_{2t}^{(1)} \approx 0$ at $c = 0$, i.e., the upper layer is so viscous that it effectively halts the horizontal motion in the lower fluid at the interface. This is the same result as given by Lamb (1932) for the inextensible limit of a thin viscous surface film.

We then obtain from (4.9):

$$\omega^2 + (1+i)g\kappa^2/(2\gamma) - g\kappa = 0 \quad (4.13)$$

where $\gamma = (\omega/2\nu_2)^{1/2}$ is connected to m by (4.5). Taking $\kappa = k + i\alpha$, where the damping rate α is assumed to be small, balance to $O(\nu_2^{1/2})$ in (4.13) yields for the real and imaginary parts, respectively:

$$\omega^2 = \omega_0^2\left(1 - \frac{k}{2\gamma}\right), \quad \omega_0^2 = gk \quad (4.14)$$

$$\alpha = \frac{k^2}{2\gamma} = \frac{\nu_2^{1/2}\omega^{7/2}}{2^{1/2}g^2}. \quad (4.15)$$

The last result also follows from Lamb's calculation if we connect spatial decay α and temporal decay β through the group velocity c_g, such that $\alpha = \beta/c_g$ (Gaster, 1962; Phillips, 1977).

The displacement field and pressure distribution in the ocean may now be written:

$$x_2^{(1)} = \frac{k}{\omega}e^{-\alpha a}\left\{\left[e^{kc}\left(\cos\alpha c - \frac{\alpha}{k}\sin\alpha c\right)\right.\right.$$
$$\left. - e^{\gamma c}\left(\cos\gamma c + \frac{\alpha}{k}\sin\gamma c\right)\right]\cos(ka - \omega t)$$
$$+\left[-e^{kc}\left(\sin\alpha c + \frac{\alpha}{k}\cos\alpha c\right)\right.$$
$$\left.\left. - e^{\gamma c}\left(\sin\gamma c - \frac{\alpha}{k}\cos\gamma c\right)\right]\sin(ka - \omega t)\right\} \quad (4.16)$$

$$z_2^{(1)} = \frac{k}{\omega}e^{-\alpha a}\left\{\left[e^{kc}\left(\cos\alpha c - \frac{\alpha}{k}\sin\alpha c\right)\right.\right.$$
$$\left. - \frac{k}{2\gamma}e^{\gamma c}\left(\left(1 - \frac{2\alpha}{k}\right)\cos\gamma c + \left(1 + \frac{2\alpha}{k}\right)\sin\gamma c\right)\right]$$
$$\times\sin(ka - \omega t) + \left[e^{kc}\left(\sin\alpha c + \frac{\alpha}{k}\cos\alpha c\right)\right.$$
$$\left. - \frac{k}{2\gamma}e^{\gamma c}\left(\left(1 + \frac{2\alpha}{k}\right)\cos\gamma c - \left(1 - \frac{2\alpha}{k}\right)\sin\gamma c\right)\right]$$
$$\left.\times\cos(ka - \omega t)\right\} \quad (4.17)$$

$$p_2^{(1)} = \mu_2\gamma k\left(\frac{\omega_0^2}{\omega^2}\right)e^{-\alpha a}\{[-e^{kc}(\cos\alpha c + \sin\alpha c)$$
$$+ e^{\gamma c}(\cos\gamma c - \sin\gamma c)]\cos(ka - \omega t)$$
$$+ [-e^{kc}(\cos\alpha c - \sin\alpha c) + e^{\gamma c}(\cos\gamma c + \sin\gamma c)]$$
$$\times\sin(ka - \omega t)\}. \quad (4.18)$$

The results presented here rest upon the assumption that the thickness of the viscous boundary layer in the ocean at the ice/ocean interface is much smaller than the wavelength, i.e. $k/\gamma \ll 1$. For waves of interest here, a typical period will be about 10 sec. Assuming a (turbulent) eddy viscosity of order 1 cm^2/s, we obtain $k/\gamma = 2\alpha/k \sim 10^{-3}$. Hence the condition $k/\gamma \ll 1$ is seen to be very well fulfilled. For a wave component $\zeta = \zeta_0 \exp[-\alpha a + i(ka - \omega t)]$ at the interface $c = 0$, we obtain from (2.3) and (4.17) that $\epsilon = \zeta_0\omega/k$ as in earlier works (Weber, 1983a,b).

5. Comparison with observational results

During recent years quite a few field studies have been aimed at determining the attenuation rate of waves in the MIZ; see the data summary by Wadhams et al. (1987). The attenuation coefficients are calculated from wave spectra obtained from wave buoys placed between the ice floes at various distances from the ice edge. All data indicate that the attenuation is larger for higher frequencies. Hence the ice pack acts as a filter yielding a systematic shift towards lower frequencies of the spectral peak as one moves inwards from the ice edge. The calculated attenuation rate (4.15) exhibits

qualitatively this increase for higher frequencies. However, in order to compare with observational results, a value for the viscosity coefficient must be assessed. A molecular value of ν_2 clearly must be ruled out since the motion in the ocean is turbulent. In the MIZ wind, waves and tidal currents will be the main sources for this turbulence. We recall that turbulent diffusion in the interior of the ocean is associated with values of the diffusion coefficients of about 1 $cm^2\ s^{-1}$. Near the surface in the open ocean where wind mixing, wave breaking and shear generated turbulence act together, values of ν_2 could range from 10^2 to 10^3 $cm^2\ s^{-1}$. Below the pack ice the conditions will be more calm, although in areas with strong tidal currents the presence of an ice covered surface may induce turbulence similar to that near a rigid bottom.

In Fig. 2 we have plotted the energy attenuation rate α_* versus wave period T from Wadhams et al. (1987). The plot is based on data from the Bering Sea obtained on 26 February 1983. The vertical error bars arise from least-squares errors in the attempt to fit the data with an exponential curve. The error bars along the period axis represent the range of periods covered by the frequency smoothing of each component. The valid range on the plot (10–21 s) indicates that wave energy outside this range was not measurable. The increase of decay rates for long periods outside this range is probably an artifact of the recording, e.g., thermal drift or sustained tilt of the wave buoy (Wadhams et al., 1987). The increase for short periods is most likely due to waves generated locally, either by wind or by floe movements. On the plot we have depicted the energy attenuation coefficient $\alpha_* = 2\alpha$ (solid line) where α is given by (4.15). Here we are taking $\nu_2 = 4$ $cm^2\ s^{-1}$. The fit with the results from the observational data is very good within the valid range.

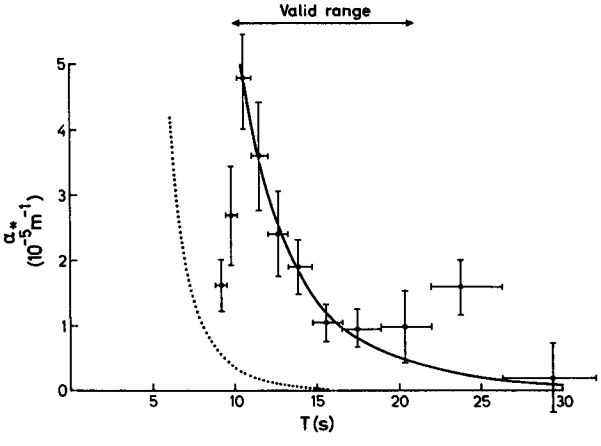

FIG. 2. Energy attenuation rate α_* versus wave period T. The observational data are based on measurements from the Bering Sea on 26 February 1983; see Wadhams et al. (1987). The full and dotted lines are theoretical decay rates $\alpha_* = 2\alpha$, where α is given by (4.15) and (5.1) respectively, using an eddy viscosity $\nu_2 = 4$ $cm^2\ s^{-1}$.

To illustrate the effectiveness of a horizontal no-slip surface condition on wave damping, we may compare with the case of a free surface. Then the requirement of a vanishing horizontal stress [$P^{(xz)} = 0$] replaces $x_{2t}^{(1)} = 0$ at $c = 0$, leading to

$$\alpha_* = 2\alpha = \frac{8\nu_2}{g^3}\left(\frac{2\pi}{T}\right)^5; \tag{5.1}$$

see Phillips (1977). With $\nu_2 = 4$ $cm^2\ s^{-1}$ as before, this relation is plotted in Fig. 2 as a dotted curve. The obtained damping rates are much too small to account for the observed damping. In order to yield an attenuation rate at the spectral peak period (here 14 s) of the required size, one would have to assume an unrealistically high value of about 1300 $cm^2\ s^{-1}$ for the eddy viscosity.

In Fig. 3 we have displayed the results from Wadhams et al. (1987) based on data from the Greenland Sea (Kong Oscars Fjord) on 4 September 1979. According to the authors, the experimental conditions during this series of measurements were nearly ideal. The incident wave spectrum was narrow, with a peak period at 10.5 s. The valid range (energy density greater than 0.01 m^2 s) extends from about 8 to 14 s. The broken lines on the plot are decay rates from the single and multiple scattering theory of Wadhams (1973a, 1975). The solid line is the attenuation coefficient $\alpha_* = 2\alpha$ obtained from (4.15) with $\nu_2 = 20$ $cm^2\ s^{-1}$.

Finally, in Fig. 4, we compare with results from the Bering Sea, obtained in March 1979 and reported earlier by Squire and Moore (1980). With a value of $\nu_2 = 1$ $cm^2\ s^{-1}$, we note that within the valid range, our theory (solid line) gives a better fit with the data than the scattering theory of Wadhams et al. (1987) (broken lines).

When making the comparisons above, one should bear in mind that the attenuation rate (4.15) for a single wave component is obtained for a rather idealized situation, i.e., a thin, very viscous homogeneous fluid layer overlaying a slightly viscous ocean. The attenuation rates reported by Wadhams et al. (1987) are based on observational data from various places within the MIZ and cover a variety of ice conditions. They constitute, more or less, average values for the entire region. So why this apparently good fit between our theory and the observational data? It seems to be related to the more general behavior of ice floes in ocean waves. For single, thin ice floes in an inviscid ocean, Squire (1983b) has demonstrated that horizontal sway may be considerably smaller than vertical heave. This occurs for floe diameters and ocean wavelengths which typically may be found in the transition zone of the MIZ. In addition, for high ice concentrations, frequent collisions between neighboring floes will reduce the horizontal motion, so that the horizontal velocity of the ice floes in a wave field may be negligible, or at least small compared to the orbital particle velocities in the

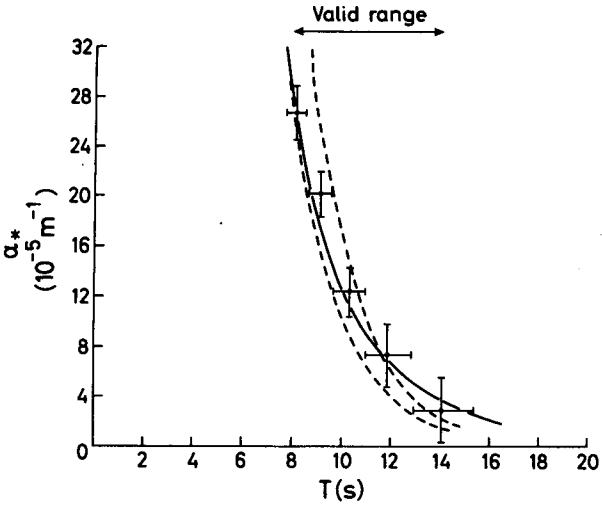

FIG. 3. Energy attenuation rate α_* versus wave period T. The observational data are based on measurements from the Greenland Sea on 4 September 1979; see Wadhams et al. (1987). The broken lines are decay rates from single and multiple scattering (Wadhams et al.). The full line represents the decay rate $\alpha_* = 2\alpha$ from (4.15) with $\nu_2 = 20$ cm^2 s^{-1}.

waves near the surface. Mathematically this leads to a no-slip condition for the horizontal velocity at the ice/water boundary, which is exactly the same condition obtained in the asymptotic limit of our theoretical model. The ice floes move more or less freely in the vertical direction. Hence a vanishing vertical stress component seems to be a reasonable approximation at the ice/water boundary. Accordingly, the mathematical problem in the case of larger, densely packed ice floes in ocean waves is identical to the asymptotic model analyzed before. The same dispersion relation and damping rate results. However, the effect of floe collisions, i.e., energy loss due to inelastic deformations, is incorporated in the parameterization of the eddy coefficient ν_2 in the water. Since the number of collisions depends on the ice concentration, this parameter is also embedded in ν_2.

6. Mean drift currents

To obtain mean drift currents in the ocean below the ice, the computations must be carried on to $O(\epsilon^2)$. The "mean," denoted by an overbar, is taken to represent time average over one wave period $T = 2\pi/\omega$. The equations governing the mean drift are given in Pierson (1962) for a nonrotating fluid. However, since they contain some inaccuracies, we state them here in corrected form, including rotation. For the mean momentum we find:

$$-\bar{x}_{tt}^{(2)} + f\bar{y}_t^{(2)} + \nu\nabla_L^2\bar{x}_t^{(2)} = \overline{\Pi}_a^{(2)} - \frac{1}{\rho}\overline{p_a^{(1)}x_a^{(1)}} - \frac{1}{\rho}\overline{p_c^{(1)}z_a^{(1)}} + \nu[2\overline{x_a^{(1)}x_{taa}^{(1)}} + 2\overline{z_c^{(1)}x_{tcc}^{(1)}} + 2\overline{z_a^{(1)}x_{tac}^{(1)}} + 2\overline{x_c^{(1)}x_{tac}^{(1)}} + \overline{x_{ta}^{(1)}\nabla_L^2x^{(1)}} + \overline{x_{tc}^{(1)}\nabla_L^2z^{(1)}}] \quad (6.1)$$

$$-\bar{y}_{tt}^{(2)} - f\bar{x}_t^{(2)} + \nu\nabla_L^2\bar{y}_t^{(2)} = 0 \quad (6.2)$$

$$-\bar{z}_{tt}^{(2)} + \nu\nabla_L^2\bar{z}_t^{(2)} = \overline{\Pi}_c^{(2)} + g(\overline{x_a^{(1)}z_c^{(1)}} - \overline{x_c^{(1)}z_a^{(1)}}) - \frac{1}{\rho}\overline{p_a^{(1)}x_c^{(1)}} - \frac{1}{\rho}\overline{p_c^{(1)}z_c^{(1)}} + \nu[2\overline{x_a^{(1)}z_{taa}^{(1)}} + 2\overline{z_c^{(1)}z_{tcc}^{(1)}} + 2\overline{z_a^{(1)}z_{tac}^{(1)}} + 2\overline{x_c^{(1)}z_{tac}^{(1)}} + \overline{z_{ta}^{(1)}\nabla_L^2x^{(1)}} + \overline{z_{tc}^{(1)}\nabla_L^2z^{(1)}}]. \quad (6.3)$$

Here we have defined $\Pi^{(2)} = p^{(2)}/\rho + gz^{(2)}$, which constitutes the effective pressure per unit density. Furthermore, we assume that there is no external horizontal pressure gradient in the problem. Here and from now on, we drop the subscript 2; this should not lead to any confusion, since hereafter we only need consider the lower fluid (the ocean).

In the vertical the mean velocity and accelerations are very small. The effective pressure $\overline{\Pi}^{(2)}$ is obtained to the required accuracy from (6.3) by neglecting the terms on the left-hand side.

As in Weber (1983a,b) we define horizontal mean flow components

$$u = \epsilon^2\bar{x}_t^{(2)}, \quad v = \epsilon^2\bar{y}_t^{(2)}, \quad (6.4)$$

and a complex drift velocity $W = u + iv$. By computing the right-hand side of (6.1), where $\overline{\Pi}_a^{(2)}$ is obtained from (6.3), the mean drift equation finally reduces to

$$\nu W_{cc} - W_t - ifW = \nu\zeta_\delta^2\omega k^3 e^{-2\alpha a}\left(4e^{2kc} + \frac{4\gamma^2}{k^2}e^{\gamma c}\sin\gamma c + \frac{3\gamma^2}{k^2}e^{2\gamma c}\right). \quad (6.5)$$

Here we have utilized the fact that $\partial^2/\partial c^2 \gg \partial^2/\partial a^2$.

We assume that the ice is relatively closely packed and has a negligible motion along the wave slope. Hence, from a tangential no-slip condition the mean horizontal drift current to $O(\epsilon^2)$ at the ice/water interface may be written

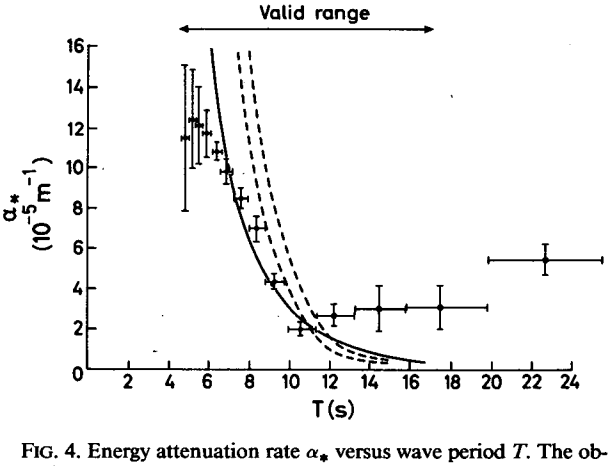

FIG. 4. Energy attenuation rate α_* versus wave period T. The observational data are based on measurements from the Bering Sea, March 1979 (Squire and Moore, 1980). The broken and full lines are as in Fig. 3 except with $\nu_2 = 1$ cm^2 s^{-1}.

$$\bar{x}_t^{(2)} = -\overline{z_t^{(1)} z_a^{(1)}}, \quad \bar{y}_t^{(2)} = 0 \quad \text{at} \quad c = 0,$$

or, from (4.17) and (6.4)

$$W = \frac{1}{2}\zeta_0^2 \omega k e^{-2\alpha a}, \quad c = 0. \tag{6.6}$$

In the deep ocean the drift current is assumed to vanish, i.e.

$$W \to 0, \quad c \to -\infty. \tag{6.7}$$

The drift problem defined by (6.5)–(6.7) has much in common with those studied by Madsen (1978), Weber (1983a,b) and Jenkins (1986) for a free surface. However, due to the no-slip condition applied here at the upper boundary, the viscous effects become much more pronounced. For a discussion of the nonrotating case, the reader is referred to Craik (1982). In that paper, which considers waves on a contaminated surface, the mean drift gradient is taken to vanish at the surface, with important consequences for the development of the drift solution, as will be discussed later.

Since the wave problem does not start from rest, it is not obvious which initial condition should be applied for the mean drift. For surface waves the wave drift along the propagation direction will establish itself very quickly, while the deflection due to the earth's rotation will occur on a much larger time scale. Therefore, we take as initial condition:

$$W = \zeta_0^2 \omega k e^{2(kc - \alpha a)}, \quad t = 0, \tag{6.8}$$

i.e., the spatially modulated classic Stokes drift.

We introduce Stokes and Ekman depths $L = 1/(2k)$ and $D = (2\nu/f)^{1/2}$, respectively, which naturally arise in this kind of problem (Weber, 1983a,b). By Laplace transforms a solution to (6.5)–(6.8) may be written:

$$\begin{aligned} W = \zeta_0^2 \omega k e^{-2\alpha a} \Bigg\{ & \frac{1+2iq}{1+4q^2} e^{c/L} + \frac{3+28q^2-8iq}{4(1+4q^2)} e^{(1+i)c/D} \\ & - 2e^{\gamma c}\cos\gamma c + \frac{3}{4}e^{2\gamma c} + \frac{e^{-ift}}{\pi}\int_0^\infty \Bigg[-\left(\frac{2q(2q-i)}{1+4q^2}\right) \\ & \times \frac{1}{\xi + 4k^2\nu} + \left(\frac{3+28q^2-8iq}{4(1+4q^2)}\right)\frac{1}{\xi + if} - \frac{2\xi}{\xi^2+\omega^2} \\ & + \frac{3}{4(\xi+2\omega)}\Bigg] e^{-\xi t}\sin(c\xi^{1/2}/\nu^{1/2})\,d\xi \Bigg\} \end{aligned} \tag{6.9}$$

where $q = L^2/D^2$. In this solution the four first terms on the right-hand side represent the steady part. The integral on the right tends to zero as $t \to \infty$. It describes the approach towards the steady state through damped inertial oscillations.

We introduce a nondimensional drift velocity W_* and a nondimensional vertical coordinate c_* by taking

$$W = \zeta_0^2 \omega k e^{-2\alpha a} W_*, \quad c = -Lc_*. \tag{6.10}$$

In Fig. 5 we have displayed a hodograph of the steady nondimensional solution $W_*^{(s)} = W_*$ $(t \to \infty)$ from (6.9) and (6.10). The crosses and numbers on the curve represent nondimensional depths defined by (6.10). In this example we have taken $\nu = 10$ cm^2 s^{-1}, $f = 1.38\ 10^{-4}$ s^{-1} and $T = 2\pi/\omega = 10$ s, which are fairly typical values for these parameters in the MIZ. This gives $\gamma^{-1} = 0.06$ m, $D = 3.8$ m and $L = 12.4$ m for the characteristic length scales of the problem. The reader is reminded of the fact that the waves propagate in the positive x (or u_*) direction. Having used the sign for f for the Northern Hemisphere, we note the characteristic spiraling of the drift vector to the right with depth. Of particular interest in this problem is the pronounced velocity maximum in the viscous boundary layer just below the ice (the effective dimensionless boundary-layer thickness $\delta = \pi(\gamma L)^{-1}$ is 0.014 in the present example). In this thin layer the effect of rotation is very small, as seen from the direction of the drift vector. The maximum nondimensional mean drift velocity in the wave direction is about 1.8, a substantial increase as compared to the inviscid nondimensional Stokes drift, which is very near 1 in this region. In general it can be shown from (6.9) and (6.10) that the steady solution $W_*^{(s)}$ reduces to

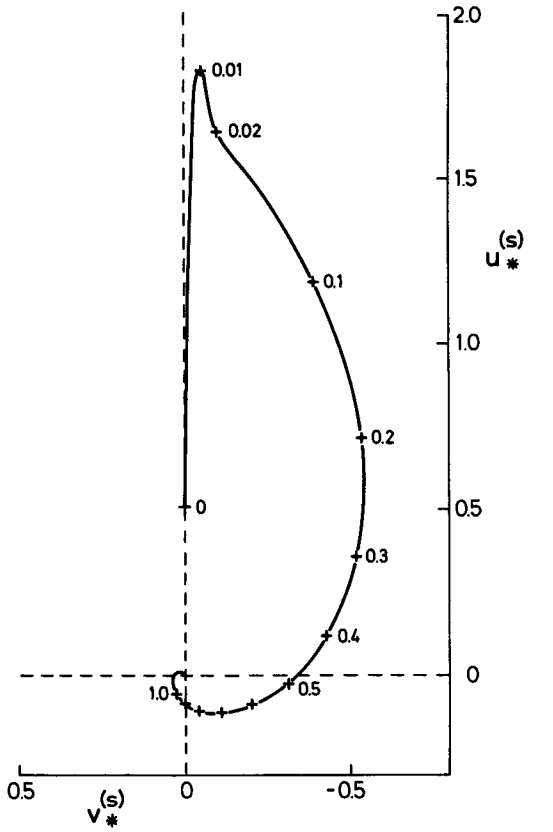

FIG. 5. Hodograph of the steady nondimensional drift current defined by (6.10). The crosses and numbers on the plot represent nondimensional depths. The waves propagate in the positive x-direction. See the text for details.

$$\left.\begin{aligned} u_*^{(s)} &= \frac{7}{4} + \mathrm{O}[k/\gamma, (f/\omega)^{1/2}] \\ v_*^{(s)} &\sim \mathrm{O}[k/\gamma, (f/\omega)^{1/2}] \end{aligned}\right\} \qquad (6.11)$$

at $c_* = \delta$, i.e., at the outer edge of the surface boundary layer. The parameters k/γ and f/ω are very small, according to earlier assumptions.

The increase in drift velocity discussed above is due to diffusion of mean horizontal momentum from the boundary $c = 0$. Essentially it arises from the lack of ability of the viscosity-modified Stokes drift to satisfy the boundary condition (6.6) along the sloping surface. This phenomenon is a surface parallel to the famous result of Longuet-Higgins (1953) for waves in a channel of finite depth. He demonstrates the existence of a forward bottom jet exceeding the inviscid Stokes drift just outside the boundary layer by a factor of 5/2, when the mean horizontal pressure gradient is set equal to zero; see also Phillips (1977, Eqn. 3.4.27).

In Fig. 6 we have plotted the transient development of the nondimensional mean drift current from (6.9) and (6.10) at four different values of c_*: 0.02, 0.1, 0.4 and 1.6. The values of the physical parameters are the same as in Fig. 5. The dots and numbers on the plot denote time in pendulum hours after the onset of streaming motion. We notice the deflection to the right of the initial drift direction, and the characteristic clockwise spiraling towards a steady state (marked by a cross) at each particular depth. The period of half a pendulum day is clearly seen for these damped inertial oscillations.

At $c_* = 0.02$, which is close to the outer edge of the surface boundary layer, the influence of viscosity is strong. The inertial motion is effectively suppressed and the drift vector approaches its steady value quite rapidly. At some larger depth, $c_* = 0.1$, the presence of the surface layer is still felt. This is obvious from the small amplitude of the damped inertial oscillations at that depth and the fact that the drift vector is fairly close to its steady value after half a pendulum day or so. At larger depths the damping is less pronounced, and the situation is more like the one obtained for wave drift when the upper surface is stress-free (Weber, 1983b; Jenkins, 1986). For $c_* = 0.4$ the oscillating adjustment towards the steady state will continue for several pendulum days. At even larger depths, here represented by $c_* = 1.6$, the steady-state drift practically vanishes, as also seen from Fig. 5. The initial nondimensional Stokes drift of 0.2 at this depth will trigger off inertial oscillations which will persist for a very long time.

The development in time described here will be qualitatively repeated for other choices of the physical parameters. It should be mentioned, however, that the speed of progress towards the steady state very much depends on the value of the eddy viscosity (Weber, 1983b; Jenkins, 1986).

Finally, we shall remark on the dynamic conditions

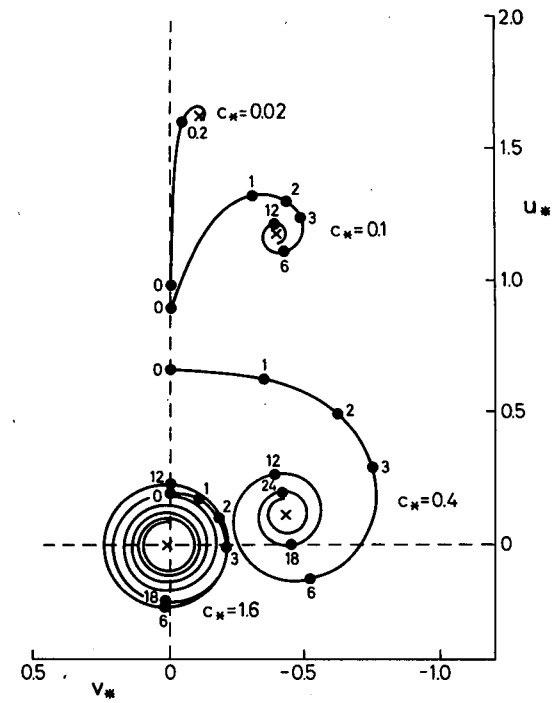

FIG. 6. Hodograph of the transient nondimensional drift current at dimensionless depths $c_* = 0.02, 0.1, 0.4, 1.6$. The dots and numbers on the plot denote time in pendulum hours. The choice of the physical parameters is the same as in Fig. 5. See the text for details.

at the boundary $c = 0$. If one assumes that the vertical *gradient* of the mean drift velocity vanishes at $c = 0$, a large virtual wave stress is imposed at the upper boundary, if the primary wave field, as here, is constrained by a vanishing horizontal velocity at $c = 0$. This may eventually result in a large increase of the drift velocity also in the interior of the fluid; see Craik (1982) for the nonrotating case. Craik's boundary condition, arising from the assumption of zero mean shear stress at the interface, may be relevant for a surface covered by a very thin layer of contaminating material such as oil or a detergent. However, for an ice covered ocean there certainly must exist a nonzero mean viscous stress between the ocean and the ice. In this case prescribed mean velocities at the boundary (here taken to be zero in the tangential direction) will constitute the relevant boundary condition.

7. Mean viscous drag on the ice

It is of considerable interest to assess the role of incoming waves in packing the ice. Observations indicate that some reflection of waves always occurs at the ice edge. This reversal of direction of wave momentum is associated with a pressure force at the ice edge acting in the direction of the wave propagation. Also wave scattering within the ice, as reported by Wadhams et al. (1986), will tend to push the ice floes together. Little

effort has been made in calculating the mean viscous drag from the waves on the ice.

We note from (6.5) and the full set of boundary conditions in Weber (1985) that the dominating stress component in the present case is along x. Denoting the corresponding drag component by $\tau_i^{(x)}$, we have

$$\tau_i^{(x)} = -\bar{P}^{(x,z)}, \quad c = 0 \tag{7.1}$$

where $\bar{P}^{(x,z)}$ is obtained from (2.4). In this expression $\mu\epsilon^2\bar{x}_{ic}^{(2)}$ is the leading term; the others are small or vanish identically. We note from (6.5) that the boundary layer terms proportional to $\exp(\gamma c)$ and $\exp(2\gamma c)$ dominate in the viscous boundary layer near the surface as far as the mean *stresses* are concerned. Accordingly, to leading order, we obtain

$$\tau_i^{(x)} = -\mu\epsilon^2\bar{x}_{ic}^{(2)}|_{c=0} = 2^{-3/2}\rho\nu^{1/2}\zeta_0^2\omega^{3/2}k \tag{7.2}$$

where we have put $a = 0$. This means, strictly speaking, that we consider the drag at the ice edge. Since the amplitude attenuation is rather weak, however, as seen from section 5, the result (7.2) will be valid also quite some distance inwards from the edge.

As seen from (7.2), the mean viscous drag depends very much on the wave amplitude. In absence of direct measurements of wave height, the wave amplitude may be assessed from the energy spectrum. Consider the case reported by Wadhams et al. (1987) from the Greenland Sea on 4 September 1979 (displayed in their Fig. 9a). An inspection of the energy spectrum at the station nearest the ice edge reveals a significant wave height of about 1.6 m. We take the effective amplitude to be half this value. Furthermore, the peak period is seen to be about 10.5 sec. The attenuation rate for this case is plotted in our Fig. 3 and gives a good fit with the measured values when $\nu = 20$ cm^2 s^{-1}. Using the values above for the amplitude, period and eddy viscosity, we obtain from (7.2) that $\tau_i^{(x)} = 1.7$ dyn cm^{-2}.

This result may be compared with the case of wind forcing. The wind drag, based on turbulent air flow above the ice, may be written

$$\tau_a = \rho_a c_D U^2. \tag{7.3}$$

Here ρ_a is the air density, c_D the drag coefficient and U the wind speed at some specific height. The drag coefficient depends on the shape of the ice. However, for drifting, flat ice the value of c_D is not substantially different from that for an open sea; a doubling of the value is often quoted (Røed, 1983). For typical values like $\rho_a = 1.2 \times 10^{-3}$ g cm^{-3} and $c_D = 3.10^{-3}$ we find from (7.3) that a wind speed of about 7 m s^{-1} produces a wind stress $\tau_a = 1.7$ dyn cm^{-2}. Hence, the mean viscous stress on the ice from the waves in magnitude may be comparable to the size of the wind stress induced by moderate winds. On the basis of this it seems as if waves alone have a considerable influence on the ice concentration. Observations in the MIZ in cases of heavy incoming swell and negligible local winds are highly desirable to test this result.

8. Upwelling near the ice edge

We consider steady wave drift and define a complex volume flux M per unit width by

$$M = \int_{-\infty}^{0} W dc. \tag{8.1}$$

Since the drift current decays rather quickly with depth, the transport M is confined to a relatively thin surface layer.

In the open sea, far away from lateral boundaries, it is straightforward to show for spatially attenuated waves [Jenkins, 1986, Eqn. (4.6)], that

$$M = M_0 = -\frac{i\eta_0^2\omega}{4q}, \quad a = 0 \tag{8.2}$$

where again $q = L^2/D^2 = f/(8\nu k^2)$. Here, η_0 is the wave amplitude in the open sea. The result above is based on the assumption of a stress-free ocean surface. We note from (8.2) that M_0 is directed at right angles to the wave propagation direction.

For the flux below an ice covered sea we obtain from (6.9):

$$M = M_i = \frac{\zeta_0^2\omega e^{-2\alpha a}}{16q^{1/2}(1+4q^2)}(A - iB) \tag{8.3}$$

where

$$A = 3 + 8q^{1/2} - 8q + 28q^2$$

$$B = 3 + 8q - 16q^{3/2} + 28q^2.$$

It is a simple exercise to show that $A > 0$, $B > 0$ for all possible values of q. Hence, the volume flux under the ice has a positive component *along* the wave propagation direction as well as a component at right angles to this direction. Due to a possible reflection of waves from the ice edge, we expect $\zeta_0 \leqslant \eta_0$. Also the eddy viscosity ν may attain different values in the open sea and under the ice. However, the important point here is that a *difference* exists in volume transports in the direction normal to the ice edge. Since this flux component vanishes in the open sea and is nonzero (and positive) under the ice, upwelling of water from below inevitably must occur near the ice edge. The vertical velocity associated with this upwelling is difficult to assess. It depends on the width of the area where this process occurs and cannot be determined from the present analysis.

It has been recognized for some time (Gammelsrød et al., 1975) that upwelling may occur near the ice edge due to discontinuity in the wind stress. Upwelling in this region is also evident from field observations (Buckley et al., 1979). Gammelsrød et al. considered a stationary ice edge. In that problem wind forcing may create an off-ice Ekman transport that is not met by a similar transport below the ice-covered region.

This divergence drives the upwelling. The present problem is analogous, but here the (wave-induced) transport *under the ice* is not met by a similar transport in the open ocean. The result is the same, however; an upwelling driven by the divergence in the horizontal transport. The present result is also based on the assumption that the motion of the ice is negligible, or at least small compared to the mean drift velocity in the water. Røed and O'Brien (1983) have demonstrated that the ocean response at the ice edge, i.e., whether upwelling or downwelling occurs, is linked to the motion of the ice edge under wind action. A moving ice cover will probably also modify the present results. Our study indicates, however, that the effect of wave-induced drift should be incorporated in more elaborate ice–ocean interaction models.

Finally, a mean vertical drift always must occur when the horizontal wave drift decays horizontally. Denoting the vertical drift by w, we obtain from (2.2) that

$$w_c = -u_a = 2\alpha u \tag{8.4}$$

where u is given by the real part of (6.9). However, since the spatial attenuation coefficient α is so small, the vertically induced flow obtained from (8.4) will in most practical cases be negligible.

9. Summary and concluding remarks

When surface gravity waves penetrate an area covered by packed ice floes their amplitudes attenuate. This attenuation has been investigated theoretically using a Lagrangian description of motion. The individual ice floes are assumed to be very small and so closely packed that they form a soupy ice-agglomeration. This agglomeration is treated as a viscous Newtonian fluid. The ocean is deep, viscous and rotating. There is no wind in the problem, and the ice-agglomeration layer is assumed to be at rest. We show that in the asymptotic limit of a very viscous, thin upper layer the horizontal boundary condition at the ice–ocean interface essentially reduces to that of a vanishing horizontal velocity.

Reasonable values for the eddy viscosity in the present theory give attenuation rates which fit well with observations from more general ice conditions in the MIZ. The reason for this appears to be that closely packed larger ice floes to a good approximation act as a horizontally motionless lid as far as incoming waves are concerned. In applying the theory to more general ice conditions, the effect of floe collisions, which again depends on the ice concentration, is embedded in the numerical value of the eddy coefficient.

From nonlinear theory we compute the drift current under the ice and discuss its temporal and spatial variations. Of particular interest is the strong jetlike behavior in the viscous boundary layer near the ice–ocean interface.

Furthermore, we compute the viscous drag on the ice induced by the wave motion. This drag acts essentially in the wave propagation direction. It may, under certain circumstances, be comparable in magnitude to the frictional drag induced by the wind. This means that the waves alone (e.g., swell) are capable of packing the ice. Additional packing will result from reflection of waves from the ice edge and scattering of waves within the ice pack (Wadhams, 1973a, 1975).

A comparison between integrated horizontal transports in the open ocean and under the ice has been made. It shows that the flux component in the wave propagation direction is zero in the open ocean and nonzero (and positive) under the ice. This must lead to upwelling of water in the vicinity of the ice edge. The packing of the ice due to a mean viscous drag develops rather quickly (on a time scale associated with turbulent vertical diffusion of momentum). Upwelling, as described here, will occur on a much larger time scale; typically larger than the inertial period. This is of importance, since the incoming wave field always has a finite duration time.

The results here for a single wave component may easily be extended to a random wave field. By averaging over a period long enough to eliminate low-frequency oscillations due to interference of wave components closely spaced in frequency, the total mass transport becomes the vector sum of the individual contributions from each wavenumber (Chang, 1969; Jenkins, 1986). Furthermore, a directional wave spectrum may, through nonlinear interactions, give rise to interesting spatial variations of the flow pattern in the surface layer (Weber, 1985). The phenomenon is analogous to acoustic streaming, and the strength of the circulation of the roll motion will here be enhanced. This is due to the increased influence of viscosity near the surface in the present problem.

The MIZ is a very interesting area not only because of its importance for the marine biological production and its impact on the climate, but also because the future increasing demand for oil will push offshore drilling activity further into subpolar and polar regions. An adequate understanding of the dynamics of the MIZ is required for the planning and execution of such operations. Most of the present dynamical models of the MIZ are concerned with wind forcing only. The results of this paper show that the effect of swell and wind sea must be included in such models.

Acknowledgments. This research was carried out while the author was visiting the Department of Applied Mathematics and Theoretical Physics, University of Cambridge, UK. The paper has benefited from discussions with Dr. V. A. Squire of Scott Polar Research Institute. His help is gratefully acknowledged. The visit was made possible by a Hambro Fellowship awarded by Clare Hall, Cambridge, and a research fellowship granted by the Royal Norwegian Council for Scientific and Industrial Research (NTNF).

REFERENCES

Buckley, J. R., T. Gammelsrød, J. A. Johannessen, O. M. Johannessen and L. P. Røed, 1979: Upwelling: Oceanic structure at the edge of the Arctic ice pack in winter. *Science,* **203,** 165–167.

Chang, M.-S., 1969: Mass transport in deep-water long-crested random gravity waves. *J. Geophys. Res.,* **74,** 1515–1536.

Craik, A. D. D., 1982: The drift velocity of water waves. *J. Fluid Mech.,* **116,** 187–205.

Gammelsrød, T. A., M. Mork and L. P. Røed, 1975: Upwelling possibilities at an ice edge, homogeneous model. *Mar. Sci. Commun.,* **1,** 115–145.

Gaster, M., 1962: A note on the relation between temporally increasing and spatially increasing disturbances in hydrodynamic stability. *J. Fluid Mech.,* **14,** 222–224.

Jenkins, A., 1986: A theory for steady and variable wind and wave induced currents. *J. Phys. Oceanogr.,* **16,** 1370–1377.

Lamb, H., 1932: *Hydrodynamics.* 6th ed., Cambridge University Press.

Longuet-Higgins, M. S., 1953: Mass transport in water waves. *Phil. Trans. Roy. Soc. London,* **A245,** 535–581.

Madsen, O. S., 1978: Mass transport in deep water waves. *J. Phys. Oceanogr.,* **8,** 1009–1015.

Martin, S., and P. Kauffman, 1981: A field and laboratory study of wave damping by grease ice. *J. Glaciol.,* **27,** 283–313.

Phillips, O. M., 1977: *Dynamics of the Upper Ocean.* 2nd ed., Cambridge University Press.

Pierson, W. J., 1962: Perturbation analysis of the Navier–Stokes equations in Lagrangian form with selected linear solutions. *J. Geophys. Res.,* **67,** 3151–3160.

Røed, L. P., 1983: Sensitivity studies with a coupled ice–ocean model of the marginal ice zone. *J. Geophys. Res.,* **88,** 6039–6042.

——, and J. J. O'Brien, 1983: A coupled ice–ocean model of upwelling in the marginal ice zone. *J. Geophys. Res.,* **88,** 2863–2872.

Squire, V. A., 1978: Dynamics of ocean waves in a continuous sea ice cover. Ph.D. dissertation, University of Cambridge, 191 pp + plates.

——, 1983a: Dynamics of ice floes in sea waves. *J. Soc. Underwater Technol.,* **9**(1), 20–26.

——, 1983b: Numerical modelling of realistic ice floes in ocean waves. *Ann. Glaciol.,* **4,** 277–282.

——, 1984: Sea ice. *Sci. Prog. Oxf.,* **69,** 19–43.

——, and S. C. Moore, 1980: Direct measurement of the attenuation of ocean waves by pack-ice. *Nature,* **283,** 365–368.

Wadhams, P., 1973a: The effect of a sea ice cover on ocean surface waves. Ph.D. dissertation, University of Cambridge, 223 pp.

——, 1973b: Attenuation of swell by sea ice. *J. Geophys. Res.,* **78,** 3552–3563.

——, 1975: Airborne laser profiling of swell in an open ice field. *J. Geophys. Res.,* **80,** 4520–4528.

——, V. A. Squire, D. J. Goodman, A. M. Cowan and S. C. Moore, 1987: The attenuation of ocean waves in the marginal ice zone. *SPRI Tech. Rep. 87-1,* University of Cambridge, (in press).

Weber, J. E., 1983a: Steady wind- and wave-induced currents in the open ocean. *J. Phys. Oceanogr.,* **13,** 524–530.

——, 1983b: Attenuated wave-induced drift in a viscous rotating ocean. *J. Fluid Mech.,* **137,** 115–129.

——, 1985: Friction-induced roll motion in short-crested surface gravity waves. *J. Phys. Oceanogr.,* **15,** 936–942.

——, 1987: Eulerian versus Lagrangian approach to wave drift in a rotating ocean. Vetenskaps och Vitterhetssamhället, Göteborg. *Acta. Ser. Geophys.,* **4,** (in press).